Journal of Nuclear Materials 425 (2012) 76–82

Contents lists available at SciVerse ScienceDirect

Journal of Nuclear Materials

journal homepage: www.elsevier.com/locate/jnucmat

Experimental study of the nucleation and growth of *c*-component loops under charged particle irradiations of recrystallized Zircaloy-4

L. Tournadre [a,*], F. Onimus [a], J.-L. Béchade [a], D. Gilbon [b], J.-M. Cloué [c], J.-P. Mardon [c], X. Feaugas [d], O. Toader [e], C. Bachelet [f]

[a] CEA–DEN, Section for Applied Metallurgy Research, 91191 Gif-sur-Yvette, Cedex, France
[b] CEA–DEN, Nuclear Material Department, 91191 Gif-sur-Yvette, Cedex, France
[c] AREVA NP SAS Fuel Business Unit 10, Rue Juliette Recamier 69456, Lyon Cedex 06, France
[d] Laboratoire d'Etude des Matériaux en Milieux Agressifs (LEMMA), Université de La Rochelle, 17042 La Rochelle Cedex 1, France
[e] Michigan Ion Beam Laboratory (MIBL), University of Michigan, Ann Arbor, MI 48109, USA
[f] Centre de Spectrométrie Nucléaire et de Spectroscopie de Masse (CSNSM), Université Paris-Sud 11, 91405 Orsay Campus, France

ARTICLE INFO

Article history:
Available online 3 December 2011

ABSTRACT

Recrystallized zirconium alloys, used as structural materials for the Pressurized Water Reactor fuel assembly, undergo under neutron irradiation induced stress free growth which accelerates for high irradiation doses. This acceleration is correlated with the formation of *c*-component vacancy dislocation loops in the basal plane. Since these defects are responsible for breakaway growth of recrystallized zirconium alloys, it is of prime importance to know the various factors that can affect their nucleation and growth. In the present work, two types of charged particle irradiations were conducted on recrystallized Zircaloy-4 samples in order to study *c*-component loops. A 2 MeV proton irradiation was performed up to a dose of 11.5 dpa at 623 K, and 600 keV Zr ion irradiations were carried out at 573 K up to 7 dpa. For the first time after those charged particle irradiations, *c*-component loops were observed by Transmission Electron Microscopy. It has been shown that under Zr ion irradiation they start to nucleate and grow beyond a threshold dose as for neutron irradiation. The differences in the *c*-component loop microstructure are discussed for both ion irradiations and compared to the microstructure observed after neutron irradiation. Furthermore, it is shown that after proton irradiation the irradiated layer exhibits a misfit strain which is consistent with the irradiation induced growth of recrystallized zirconium alloys.

1. Introduction

Zirconium alloys, such as Zircaloy-4, are used as cladding and structural material for the fuel assembly of Pressurized Water Reactor (PWR). During in-reactor normal operation, the length of the PWR fuel assembly increases with increasing fast neutron fluence. The elongation of the recrystallized Zircaloy-4 guide tubes is the result of three different phenomena: the thermal creep, the irradiation creep and the stress free growth [1,2]. The stress-free growth phenomenon corresponds to an elongation along the basal plane of the hexagonal closed packed structure and a shortening along the *c*-axis, the volume remaining constant [3]. Due to the strong texture of zirconium tubes [4], the growth of the hexagonal closed packed grains at the microscopic scale, leads to a macroscopic elongation along the axial direction of the tubes. For recrystallized zirconium alloys, at high fluence, typically after an incubation dose of 4.0×10^{25} n.m^{-2} ($E > 1$ MeV) [5], the growth rate increases. The incubation dose corresponds approximately to a damage of 6 dpa (displacements per atom). This acceleration is often referred to as "breakaway growth".

The accelerated growth rate and the incubation dose are strongly influenced by the irradiation temperature [6,7] but specimen purity is also a critical factor [8,9]. Since this phenomenon can have a significant impact on the performance of the fuel assembly a good knowledge and prediction of this breakaway growth is required.

According to several authors, the breakaway growth is clearly correlated to the nucleation of a specific microstructural irradiation defect: the *c*-component dislocation loops [10]. These defects have already been observed after neutron [11,12] and electron irradiations [9,13,14] but have never been clearly observed, to our knowledge, after ion irradiations. It is nevertheless worth noticing that in the early work of Lee et al. [15], after high dose Ni-ion bombardment of Zircaloy-2, defects with *c*-component displacement field have been observed. However, this contrast probably corresponds to the so-called "corduroy contrast" [16].

The *c*-component dislocation loops, when observed after neutron irradiation, have a Burgers vector with a component along the *c*-axis given by $\underline{b} = 1/6\langle 20\bar{2}3\rangle$ [11]. They are of vacancy type

* Corresponding author. Tel.: +33 1 6908 1231; fax: +33 1 6908 7130.
E-mail address: lea.tournadre@cea.fr (L. Tournadre).

0022-3115/$ - see front matter © 2011 Elsevier B.V. All rights reserved.
doi:10.1016/j.jnucmat.2011.11.061

only and are located in the basal plane. Since these defects are responsible for the breakaway growth of recrystallized zirconium alloys, it is of prime importance to know the various factors that can affect their nucleation and growth. Consequently, a thorough experimental study of these dislocation loops has been undertaken using charged particle irradiations. Ion irradiations of a recrystallized Zircaloy-4 were conducted up to high damage doses in a temperature range 573–623 K.

In this paper, the macroscopic deflection of the proton irradiated specimens is first analyzed and discussed in terms of radiation induced growth. TEM observations of the *c*-component loops created by ion (proton and Zr ion) irradiations are described. The loop size and density measurements are presented. The results are then compared to the microstructure obtained after neutron irradiation. Finally, the effect on the $\langle c \rangle$ loop microstructure of the damage morphology, the damage rate and the free surface are discussed.

2. Experiment

2.1. Material

The studied material is recrystallized (RXA) Zircaloy-4. The chemical content is given in Table 1. Contrary to other studies [17], the specimens are not taken from a final product in the form of thin tubing or thin sheet, but from an intermediate product. This intermediate product is a thick tube which exhibits a transverse texture as shown in Fig. 1. The final heat treatment produced a recrystallized grain structure (Fig. 2) with grain diameters of 6.2 ± 0.6 μm similar to the microstructure of recrystallized Zy-4 thin tubes.

2.2. Experimental techniques

Specimens are prepared from the Zircaloy-4 RXA (Recrystallisation Annealed) thick tube in the RD–TD (Rolling Direction–Transverse Direction) plane and are irradiated with ions (Zr ions and protons) up to 11.5 dpa in a temperature range 573–623 K.

For Zr ion irradiations, the specimens are 3 mm diameter disks and 0.1 mm thick, electropolished on one surface before irradiation. The irradiated surface is then protected by a varnish and the thin foil is made by electropolishing the rear surface.

Two 600 keV Zr ion irradiations were conducted on the ARAMIS facility at CSNSM/IN2P3-Orsay at 573 K. At this energy, the heavy ion flux (Table 2) provides a high flux, and therefore, a high irradiation dose in one day. Therefore, specimens irradiated up to four different doses are available: 4.8×10^{18} ions/m^2, 6.7×10^{18} ions/m^2, 9.5×10^{18} ions/m^2 and 11×10^{18} ions/m^2. The damage profile created by 600 keV Zr ions is shown in Fig. 3. The mean damage obtained in the thickness of the 150 nm thick thin foil corresponds respectively to 2.9, 4.1, 5.5 and 7 dpa.

For proton irradiation, the specimens used are in the form of bars: 20 mm long, 2 mm wide and 1.55 mm thick. The length of the bar is oriented along the axial direction of the thick tube (Rolling Direction referred to as RD). Before irradiation, the surface parallel to the RD–TD plane is mechanically polished to a mirror finish. This surface is then irradiated by the proton beam. After irradiation, the bars are mechanically polished from the rear surface down to 0.1 mm in thickness and punched to make 3 mm disks. On the irradiated surface, around 15 μm are removed by electropolishing. Then, a varnish is applied in order to protect the irradiated side and the thin foil is made by electropolishing from the rear surface.

A 2 MeV proton irradiation was carried out on the Michigan Ion Beam Laboratory (MIBL) Tandem up to 1.2×10^{23} protons/m^2 at 623 K. The temperature is controlled by a 2D thermal camera

Table 1
Chemical composition of the recrystallized Zy-4 intermediate product (wt.%).

Alloy	Sn%	C%	Fe%	Cr%	S%	Si%	O%
RXA Zy-4	1.35	0.015	0.21	0.10	0.002	0.009	0.13

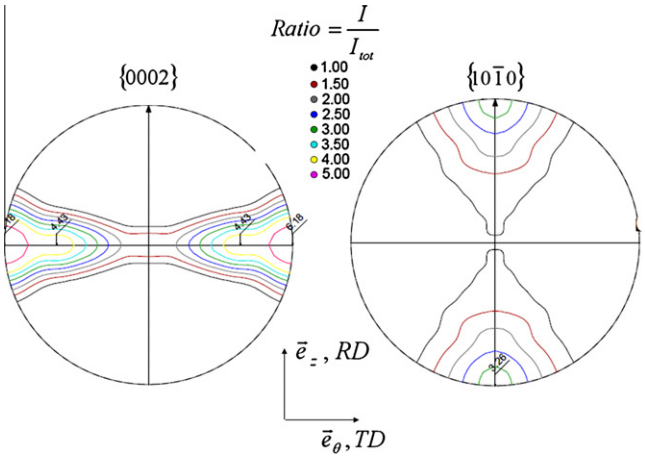

Fig. 1. {0002} and $\{10\bar{1}0\}$ pole figures, RXA Zircaloy-4.

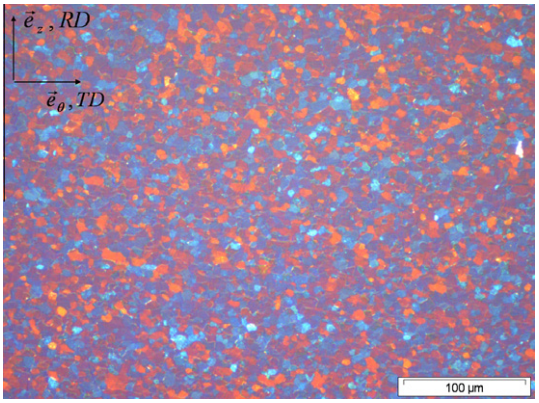

Fig. 2. Optical microscopy characterization of RXA Zircaloy-4 at mid thickness, intermediate product.

throughout the experiment. Due to the low damage rate, several days are required to reach high irradiation doses. The TRIM calculation shows (Fig. 4) that the damage peak is obtained between 25 μm and 30 μm depth whereas the damage increases only slowly between 5 μm up to 20 μm depth. The thin foils are prepared between 15 and 20 μm under the surface. The damage obtained in this region is about 11.5 dpa.

All the thin foils were prepared by electropolishing using a solution of 20% 2-Butoxyethanol and 10% perchloric acid in ethanol at temperatures around 278 K.

Transmission Electron Microscopy observations were conducted using a Philips EM 430 operating at 300 kV and a Jeol 2100 operating at 200 kV. The *c*-component dislocation loops are clearly observed when the diffraction vector is parallel to the $\langle c \rangle$ axis: $g = \langle 0002 \rangle$. Indeed, in these specific diffraction conditions, all the crystalline defects with $\langle a \rangle$ Burgers vector, such as the numerous $\langle a \rangle$ loops, are invisible. Therefore, the *c*-component loops can then be easily observed. They appear as short segments, since they are imaged edge-on. Thanks to the specific texture of the thick tube used, the majority of the grains have their $\langle c \rangle$ axis included in

Table 2
Charged particle irradiation conditions.

Facility	Particle	Energy	Temperature (K)	Damage (dpa)	Damage rate (dpa s^{-1})
ARAMIS	Zr^+	600 keV	573	2.9	5.15×10^{-4}
ARAMIS	Zr^+	600 keV	573	4.1	5.15×10^{-4}
ARAMIS	Zr^+	600 keV	573	5.5	5.15×10^{-4}
ARAMIS	Zr^+	600 keV	573	7	5.15×10^{-4}
MIBL tandem	H^+	2 MeV	623	11.5	1.43×10^{-5}

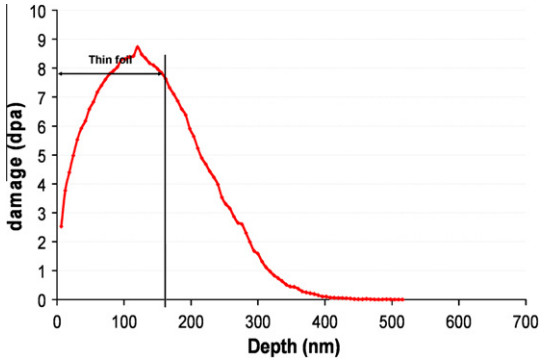

Fig. 3. TRIM calculations for 600 keV Zr ions in Zr, 11×10^{18} ions/m^2(E_d = 40 eV).

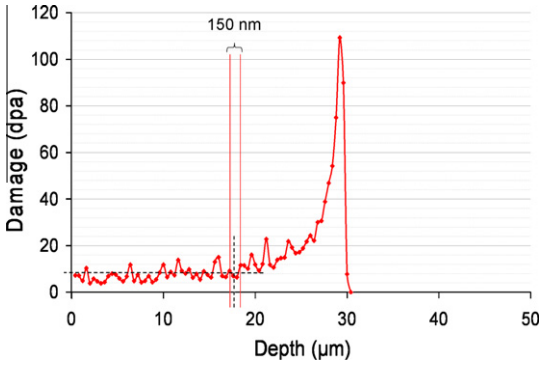

Fig. 4. TRIM calculations for 2 MeV protons in Zr, 1.2×10^{23} protons/m^2, (E_d = 40 eV).

the thin foil plane and are therefore well orientated to observe ⟨*c*⟩ loops.

TEM micrographs are taken of the entire surface of each grain studied. On these pictures the ⟨*c*⟩ dislocation loops, in the form of short segments, are manually selected. The image is then digitalized and analyzed using the Analysis 5 software.

3. Results

3.1. Proton irradiated materials

When removed from the polishing stand, the thin strips of 0.1 mm thick obtained after mechanical polishing of the proton irradiated bars exhibit a macroscopic deflection between 0.1 and 0.2 mm. This bending is measured between the top of the curvature, on the inner surface, and the line drawn between the two ends of the strip (Fig. 5a). It has to be underlined that the irradiated surface is the convex side (upper side on Fig. 5a).

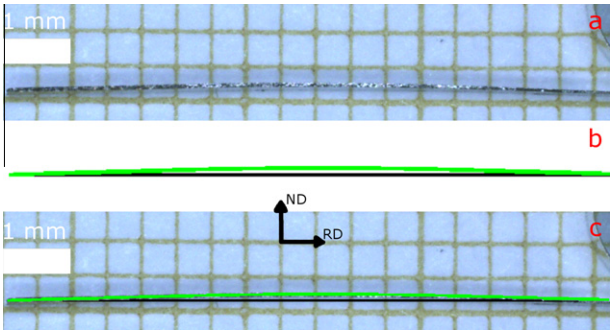

Fig. 5. (a) Thin strip bending; (b) deflection simulated by using Finite Element Method computations and (c) comparison between simulation and experiment.

This bending can probably be attributed to irradiation-induced deformation of the irradiated layer. In order to confirm the role of this layer, the irradiated surface was mechanically polished up to 50 μm depth on one of the samples. Then, as for the usual procedure, mechanical polishing on the rear surface was performed. This 0.1 mm thick specimen did not exhibit any bending, proving that the deflection is due to the radiation induced deformation of the irradiated layer. Although the oxide layer could also contribute to this deflection, its effect is probably negligible considering its small thickness (<20 nm). The deflection origin is analyzed in the discussion (Section 4.1).

The TEM observations of the thin foils show that *c*-component dislocation loops are present in the 2 MeV proton irradiated materials (Fig. 6). The ⟨*c*⟩ loops are large, numerous and rather homogeneously distributed throughout the grains. A higher loop density is observed around some precipitates (Fig. 6b). This phenomenon is also observed in neutron irradiated materials where it has been clearly established that iron coming from the precipitates enhances ⟨*c*⟩ loop nucleation [11,15,18,19]. The mean loop diameter is of 123 nm, whereas their density is about 1.0×10^{21} m^{-3} (if a thickness of 150 nm is considered for the thin foil). To our knowledge, it is the first time that *c*-component loops are observed in Zr alloys after proton irradiation.

3.2. Zr ion irradiated materials

TEM observations were carried out on the samples irradiated with Zr ions up to 2.9, 4.1, 5.5 and 7 dpa. The *c*-component dislocation loops are not observed after an irradiation conducted up to 2.9 dpa (Fig. 7a). By contrast, small ⟨*c*⟩ loops are present after 4.1 dpa (Fig. 7b) 5.5 dpa (Fig. 7c) and 7 dpa irradiations (Fig. 7d). The defects obtained seem to be homogeneously distributed throughout the grains (Fig. 8). To our knowledge, it is the first time that *c*-component dislocation loops are clearly observed in ion irradiated RXA Zircaloy-4. These observations also show that for 600 keV Zr ion irradiations, an incubation dose exists from which ⟨*c*⟩ loops start to nucleate and grow. Moreover, the ⟨*c*⟩ loop mean diameter and density significantly increase between 4.1, 5.5 and 7 dpa (Table 3).

3.3. Comparison of the microstructure obtained with Zr ion and proton irradiations

A qualitative comparison of the micrographs obtained using the two types of energetic particles shows that the ⟨*c*⟩ loop microstructure observed after proton irradiation is rather similar to the microstructure observed after neutron irradiation [20,21]. In contrast, for Zr ion irradiation, the loops are much smaller. However, these first observations have to be considered cautiously since the doses and the temperatures are slightly different.

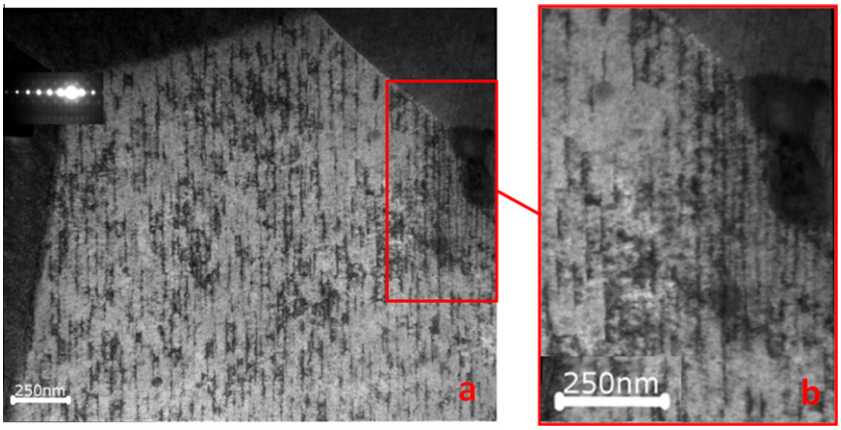

Fig. 6. (a) and (b) MIBL – proton irradiated Zircaloy-4 RXA 11.5 dpa at 623 K.

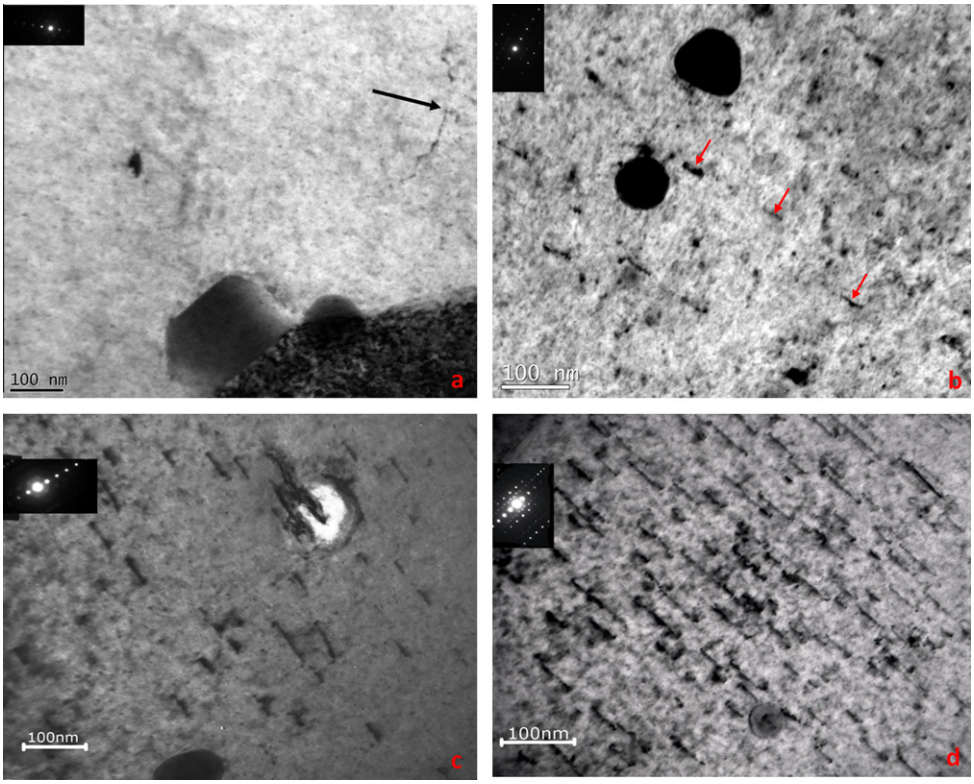

Fig. 7. ARAMIS, RXA Zircaloy-4 irradiated at 573 K (a) 2.9 dpa ($\langle c+a\rangle$ dislocation pointed in black); (b) 4.1 dpa; (c) 5.5 dpa and (d) 7 dpa.

The $\langle c\rangle$ loop diameter and density obtained with ion irradiations were carefully measured, by analyzing a large number of loops, and are reported and compared to neutron data in Table 3. Neutron damage, expressed in displacement per atom (dpa), was calculated using the conversion value given by Shishov [22].

For neutron irradiated materials, $\langle c\rangle$ loops are larger than 150 nm and, as a consequence, are truncated by the thin foil surfaces. This is why a more relevant parameter, the linear density L_v, defined by Eq. (1), has also been computed:

$$L_v = \frac{N\langle d\rangle}{V} \tag{1}$$

where N is the total number of loops, $\langle d\rangle$ the loop mean diameter and V the volume studied.

It appears that for Zr ion irradiations, $\langle c\rangle$ loops are smaller than the loops obtained by neutron irradiation. Nevertheless, the $\langle c\rangle$ loop diameter obtained with protons is comparable to the neutron values and three times larger than the diameters obtained using Zr ion. The numbers of loops per unit volume are similar for the three types of experiments.

As a consequence, the microstructure of the material irradiated with protons is closer to the microstructure obtained with neutrons. Thus, the length of loops per unit volume, L_v, obtained for proton irradiated RXA Zircaloy-4 is close to the value obtained after neutron irradiation. Moreover, after proton irradiation, $\langle c\rangle$ loop density is higher in the vicinity of some precipitates. This preferential nucleation, representative of neutron irradiation, is not observed after Zr ion irradiation. These results will be discussed in Section 4.2.

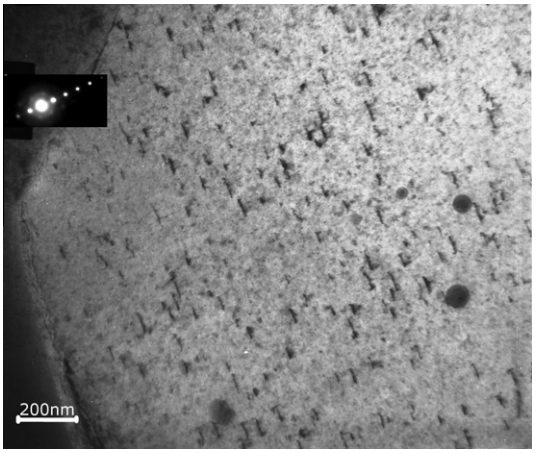

Fig. 8. RXA Zircaloy-4 irradiated by 600 keV Zr ions in the ARAMIS facility at 573 K up to 5.5 dpa. Observation performed at the same magnification than Fig. 6.

4. Discussion

4.1. Analysis of the macroscopic deflection

The macroscopic deflection of the 100 μm thick proton irradiated specimens could be explained by the radiation induced growth of the irradiated layer. Indeed, since the bar specimens are taken out from the thick tube along the Rolling Direction (RD), the $\langle 1\,0\,\bar{1}\,0\rangle$ directions of the grains are along the longitudinal direction of the strip (Fig. 5) (the Kearns factors for the *c*-axis are: $f_{RD} = 0,09$, $f_{TD} = 0,53$ and $f_{ND} = 0,38$). Therefore, a growth strain (elongation along the basal plane) results in an expansion of the irradiated layer along its length and a shortening along its width. Due to the bi-layered structure, an expansion of the irradiated layer induces a deflection of the strip along its length, the irradiated surface being convex.

In order to confirm this hypothesis, the strain of this 30 μm thick irradiated layer was estimated taking into account that the measured deflection of the strip is 0.2 mm. It is worth noted that only a zone of 10 mm long at the center of the 20 mm long strip is irradiated. Moreover, although the damage exhibits a heterogeneous profile in the irradiated layer, it is considered homogeneous, for the sake of simplicity, so that the resulting growth strain is considered to be constant in the layer in this first approach. Finally, the stress free growth phenomenon is simulated by using a thermo-elastic isotropic behavior. In that case, the growth strain is equivalent to a thermal expansion strain introduced in the irradiated layer only.

As a first approach, the Timoshenko model for a bimetallic strip was applied [24], assuming a geometry in which the entire surface is irradiated to a depth of 30 μm. Considering the symmetry, the strip was cut in the middle and reduced to a 2D geometry (Fig. 9). The Young Moduli E_1 and E_2, for the irradiated layer and for the substrate respectively, are considered to be equal in our case. In these conditions, the relationship between the curvature of the strip and the characteristics of the two layers is given by following equation:

$$\kappa = \frac{6E_1E_2t_1t_2(t_1+t_2)\varepsilon}{E_1^2t_1^4 + E_2^2t_2^4 + 4E_1E_2t_1^3t_2 + 6E_1E_2t_1^2t_2^2 + 4E_1E_2t_1t_2^3} = \frac{6t_1t_2(t_1+t_2)\varepsilon}{t_1^4 + t_2^4 + 4t_1^3t_2 + 6t_1^2t_2^2 + 4t_1t_2^3} \quad (2)$$

where κ is the strip curvature, t_1 and t_2 the thicknesses of the irradiated layer and the substrate respectively. ε is the misfit strain between the two layers. This misfit strain, or stress free strain, is attributed to the difference in expansion coefficients in the classical bimetallic strip model. The curvature κ is then related to the experimentally measured bow (d) by Eq. (3), considering that $L\kappa \ll 1$ (where L is the strip length).

$$d = \frac{\kappa L^2}{2} \quad (3)$$

Thus, to obtain a bending of about 0.2 mm, a 3.2×10^{-4} misfit strain of the irradiated layer is required.

However, it seems important to validate this first estimation by Finite Element Method computations using the CAST3M software. Indeed, Finite Element calculations allow simulating the strip behavior with a more accurate geometry for the irradiated layer. The mesh and the boundary conditions used are described schematically in Fig. 10 and a 2D geometry is adopted.

The Finite Element Method computation leads to the same result as was obtained for the first analytical approach. Indeed, a 0.2 mm bending corresponds to a 3.0×10^{-4} strain growth in the irradiated layer. The deflection obtained by simulation is drawn (Fig. 5b) and compared to the experiment (Fig. 5c).

This analysis shows that the estimated growth strain is consistent with the growth strain measured on recrystallized zirconium alloys during in-reactor experiments [25] considering its magnitude but also its orientation (elongation along the basal plane).

4.2. Discussion on the TEM observations

First of all, these new experiments demonstrate that it is possible to obtain *c*-component dislocation loops using ion (proton and Zr ion) irradiations. Indeed, to our knowledge, it is the first time that such defects have been clearly evidenced after proton and Zr ion irradiations.

Moreover, TEM observations on Zr ion irradiated specimens show that *c*-component loops start to nucleate and grow only above a threshold dose. This observation is in good agreement with the TEM observations performed after neutron irradiation [5,10,11] and also after electron irradiation [9,14].

Nevertheless, it can be pointed out, as reported in Table 3, that after Zr ion irradiations the $\langle c\rangle$ loops are smaller (24–36 nm diameter) than after neutron irradiations (>150 nm).

Table 3
RXA Zircaloy-4, characteristics of the $\langle c\rangle$ loop microstructures obtained after Zr ion, proton and neutron irradiations.

Irradiation characteristics	Damage (dpa)	Loop mean diameter (nm)	Loop density (defect/m^3)	$L_v = \frac{N\langle d\rangle}{V}$ (mm^{-3})	Number of loops analyzed
600 keV Zr ions 573 K	4.1	24 ± 3	$2.9 \times 10^{20} \pm 0.3 \times 10^{20}$	$6.6 \times 10^{12} \pm 0.8 \times 10^{12}$	639
600 keV Zr ions 573 K	5.5	27 ± 4	$6.7 \times 10^{20} \pm 0.7 \times 10^{20}$	$1.6 \times 10^{13} \pm 0.2 \times 10^{13}$	1300
600 keV Zr ions 573 K	7	36 ± 5	$9.1 \times 10^{20} \pm 0.9 \times 10^{20}$	$3.3 \times 10^{13} \pm 0.4 \times 10^{13}$	1400
2 MeV protons 623 K	11.5	123	1.0×10^{21}	1.1×10^{14}	350
PWR 583 K [20]	14	>150[a]	$<1.2 \times 10^{21}$[a]	1.8×10^{14}	
PWR 583–593 K [23]	35	>150[a]	$<1.17 \times 10^{21}$[a]	1.75×10^{14}	

[a] Values are deduced from the sample thickness.

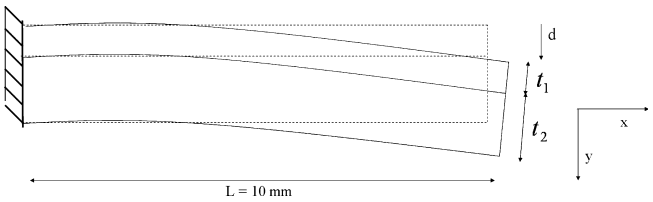

Fig. 9. Geometry for the Timoshenko resolution [24].

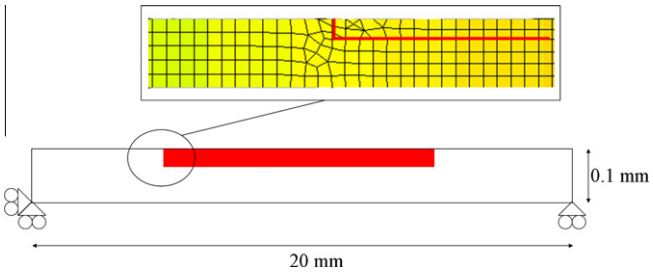

Fig. 10. Schematic representation of the bi-layer strip, boundary conditions and mesh details.

On the other hand, in the case of proton irradiation, the size (123 nm) and the linear density of loops are closer to the values obtained after neutron irradiation.

These differences in microstructure can be explained by various conflicting factors:

- First, it is known [26] that neutron or heavy ions such as Zr ions induce large displacement cascades. In these large cascades, recombination of point defects occurs, decreasing, on the one hand, the efficiency of the damage but inducing, on the other hand, small point defect clusters [27,28]. These clusters can play a significant role on the nucleation of dislocation loops such as *c*-component loops. On the contrary, proton irradiation leads to the creation of only small cascades and isolated Frenkel pairs [26]. In this respect, Zr ion irradiation is more representative of neutron irradiation than proton irradiation.
- By using Zr ion irradiation, samples are irradiated on 300 nm depth only. The free surface and the non-irradiated matrix act as sinks for point defects and thus, could influence the $\langle c \rangle$ loop microstructure. On the contrary, free surface do not affect the microstructure obtained with protons since thin foils are taken from the irradiated bulk.
- The difference in damage rate obtained between charged particle irradiation and neutron irradiation can also play a significant role on the radiation induced microstructure. Indeed, for an irradiation performed with a high damage rate the nucleation of loops is favoured at the expense of the growth leading to the creation of a high density of small loops [29]. On the other hand, for an irradiation performed with a low damage rate, it is the growth of loops which is favoured at the expense of the nucleation, leading to a low density of large loops. Moreover, a lower damage rate allows the diffusion of alloying elements, such as iron, which could lead to preferential nucleation of $\langle c \rangle$ loops around some precipitates, as observed after neutron irradiation [8,9,11].

For neutron irradiation in PWR conditions (fast neutron flux of the order of 5×10^{17} n.m^{-2} s^{-1} [22]) the damage rate is about 7.29×10^{-8} dpa/s. Thus, the damage rate is 7000 times higher using Zr ion and only 200 times higher using proton than for neutron irradiation. In this respect the proton irradiation is more representative of neutron irradiation than Zr ion irradiation.

These experiments have shown that after proton irradiation (at 623 K) the $\langle c \rangle$ loop characteristics and distributions are more similar to the $\langle c \rangle$ loop microstructures observed after neutron irradiations (at 583–593 K) than after Zr ion irradiations (at 573 K). It can therefore be concluded that the damage rate plays a major role on the $\langle c \rangle$ loop microstructures. Besides, the effect of the damage morphology seems to be not significant. Concerning the free surface, its precise role in this experiment is not clear yet [13,30] since it seems to depend on the orientation of the $\langle c \rangle$ axis. Nevertheless, since its role could not explain the lack of preferential nucleation of $\langle c \rangle$ loops around precipitates after Zr ion irradiations, it can be considered that the effect of the free surface is not significant compared to the effect of the damage rate.

However, it has to be pointed out that proton irradiation is performed at 623 K whereas Zr ion irradiation is performed at 573 K. This could also partly explain that larger loops are observed after proton irradiation [26,31]. Another reason for this observation is that the dose is slightly higher for proton irradiation than for Zr ion irradiations. A Zr ion irradiation performed at 623 K up to 11.5 dpa is therefore necessary to confirm the damage rate influence on $\langle c \rangle$ loops.

5. Conclusion

This experimental study first shows that after proton irradiation the irradiated layer exhibits a stress free strain which is consistent with the irradiation induced growth of recrystallized zirconium alloys.

But above all, this study proves for the first time, that *c*-component dislocation loops can be created in RXA Zircaloy-4 using 600 keV Zr ion and 2 MeV proton irradiations at temperature range 573–623 K. Moreover, TEM observations on Zr ion irradiated specimens show that *c*-component loops start to nucleate and grow only above a threshold dose. This observation is in good agreement with the TEM observations performed after neutron irradiations. The $\langle c \rangle$ loops created after charged particle irradiations are smaller than after neutron irradiations, and differences are larger for Zr ion irradiations than after proton irradiation. Preferential nucleation has been observed near some precipitates after proton irradiation. This phenomenon also occurs during neutron irradiations. This difference in $\langle c \rangle$ loop microstructure can mainly be explained by the high discrepancy in the damage rate between neutron and charged particle irradiations: nearly four orders of magnitude greater for Zr ions than for neutrons and only two orders of magnitude greater for protons. Thus, proton irradiation appears to be more representative of neutron irradiation than Zr ion irradiation, at least concerning $\langle c \rangle$ loops. Moreover, thanks to the high penetration depth of protons, the thin foils are taken from the bulk material. Therefore proton irradiation allows avoiding the influence of the free surface which can be a sink for point defects. Finally, the differences in the morphology of the damage (size of the displacement cascade) seem to play a minor role on the $\langle c \rangle$ loop microstructure.

Acknowledgments

The authors would like to thank AREVA NP, for the supply of the material and the financial support, S. Doriot, for the active discussion concerning $\langle c \rangle$ loops and C. Lebon for his help in Finite Element computations. For their technical assistance and their work, the authors would like to thank R. Danguillaume and B. Arnal, for specimen preparations and grain size measurements, S. Bosonnet for texture measurements and D. Hamon for chemical analysis.

To finish, the authors thank T. Vandenberghe and S. Urvoy for their help in sample preparation.

References

[1] D.G. Franklin, G. Lucas, A. Bement, ASTM STP 815 (1983) 284.
[2] D.G. Franklin, R.B. Adamson, J. Nucl. Mater. 159 (1988) 12–21.
[3] G.J.C. Carpenter, R.H. Zee, A. Rogerson, J. Nucl. Mater. 159 (1988) 86–100.
[4] C. Lemaignan, A.T. Motta, Mater. Sci. Technol. VCH 10B (1994) (Chapter 7).
[5] M. Griffiths, R.W. Gilbert, V. Fidleris, in: Zirconium in the Nuclear Industry: Eighth International Symposium, ASTM STP 1023, 1989, pp. 658–677.
[6] M. Griffiths, R.W. Gilbert, J. Nucl. Mater. 150 (2) (1987) 169–181.
[7] R.B. Adamson, R.P. Tucker, V. Fidleris, in: Zirconium in the Nuclear Industry: fifth conference, ASTM STP 754, 1982, pp. 208–234.
[8] M. Griffiths, in: Zirconium in the Nuclear Industry: fifteenth International Symposium, ASTM STP 1505, 2009, pp. 19–26.
[9] Y. De Carlan et al., in: Zirconium in the nuclear Industry: Eleventh International Symposium, ASTM STP 1295, 1996, pp. 638–653.
[10] R.A. Holt, R.W. Gilbert, J. Nucl. Mater. 137 (3) (1986) 185–189.
[11] M. Griffiths, J. Nucl. Mater. 159 (1988) 190–218.
[12] A. Jostsons, P.M. Kelly, R.G. Blake, J. Nucl. Mater. 66 (3) (1977) 236–256.
[13] M. Griffiths, M.H. Loretto, R.E. Smallman, Philosophical magazine a – physics of condensed matter structure defects and mechanical properties 49 (5) (1984) 613–624.
[14] M. Griffiths et al., J. Nucl. Mater. 208 (3) (1994) 324–334.
[15] D. Lee, E.F. Koch, J.H. Rosolows, J. Nucl. Mater. 50 (2) (1974) 162–174.
[16] W.L. Bell, J. Nucl. Mater. 55 (1) (1975) 14–22.
[17] F. Onimus et al., J. Nucl. Mater. 328 (2–3) (2004) 165–179.
[18] R.A. Holt et al., in: Zirconium in the Nuclear Industry: Twelfth International Symposium, ASTM STP 1354, 2000, pp. 86–104.
[19] S. Doriot et al., in: Zirconium in the Nuclear Industry: fourteenth International Symposium, ASTM STP 1467, 2005, pp. 175–201.
[20] D. Gilbon, C. Simonot, in: Zirconium in the Nuclear Industry: Tenth International Symposium, ASTM STP 1245, 1994, pp. 521–548.
[21] R.A. Holt, R.W. Gilbert, J. Nucl. Mater. 116 (1) (1983) 127–130.
[22] V.N. Shishov, in: Zirconium in the Nuclear Industry: fourteenth International Symposium, ASTM STP 1467, 2006, pp. 666–685.
[23] P. Bossis et al., in: Zirconium in the Nuclear Industry: fifteenth International Symposium, ASTM STP 1505, 2009, pp. 430–456.
[24] S. Timoshenko, J. Opt. Soc. Am. 11 (3) (1925).
[25] D. Gilbon et al., in: Zirconium in the nuclear industry: Twelfth International Symposium, ASTM STP 1354, 2000, pp. 51–73.
[26] G.S. Was, Fundamentals of Radiation Materials Science, Springer, 2007.
[27] F. Gao et al., J. Nucl. Mater. 294 (3) (2001) 288–298.
[28] S.J. Wooding et al., J. Nucl. Mater. 254 (2–3) (1998) 191–204.
[29] T.R. Allen et al., J. Nucl. Mater. 348 (1–2) (2006) 148–164.
[30] F. Christien, A. Barbu, J. Nucl. Mater. 346 (2–3) (2005) 272–281.
[31] C. Hellio, C.H. De Novion, L. Boulanger, J. Nucl. Mater. 159 (1988) 368–378.